Advances and Applications in Fluid Mechanics

http://www.pphmj.com
http://dx.doi.org/10.17654/FM023010025
Volume 23, Number 1, 2019, Pages 25-44 **ISSN: 0973-4686**

SIMULATION OF NATURAL CONVECTION IN BLOOD FLOW USING LATTICE BOLTZMANN METHOD

Nitin S. Bodke, Ignatius Fernandes and Neeta D. Kankane

Dr. B. N. Purandare Arts
S. S. G. G. Commerce and Science College
Lonavla, India
e-mail: bodke.nitin@gmail.com

Rosary College
Navelim, Goa, India
e-mail: ignatius4u@gmail.com

Maharashtra Institute of Technology
Pune, India
e-mail: ndkankane@gmail.com

Abstract

Lattice Boltzmann method is used to simulate natural convection in blood flow through stenotic artery. The problem of natural convection in stenotic artery is considered and the influence of elevated temperature and material properties is studied on the flow properties. A porous like square stenotic medium in a human artery with fluid (blood) at the left wall of the geometry and the north wall kept to a normalized temperature of 1.0 is considered. The flow properties like velocity profiles, streamlines, temperature profiles and

Received: April 28, 2018; Accepted: November 20, 2018

2010 Mathematics Subject Classification: 76Rxx, 76Sxx.

Keywords and phrases: Lattice Boltzmann method, porous media, non-Newtonian, blood flow, natural convection, Carreau-Yasuda model.

the rate of heat transfer are then studied with respect to the material properties like porosity and permeability and flow parameters like Rayleigh number and power law index.

Nomenclature

Symbol	Description
Da	Darcy number
Ra	Rayleigh number
ρ	Fluid density
λ_{eff}	Effective thermal conductivity
u	Volume-averaged velocity
p	Pressure
F	Total body force
ν	Shear viscosity of the fluid
G	Body force
K	Permeability
F_ε	Forchheimer's term
d_p	Solid particle diameter
ε	Porosity
τ	Relaxation time
υ	Kinematic viscosity
$g_i(x, t)$	Thermal distribution function
$g_i^{eq}(x, t)$	Equilibrium distribution function
$f_i(x, t)$	Velocity distribution function
q	Darcy flux
μ_{eff}	Effective viscosity
∇p	Pressure gradient
L	Characteristic length

1. Introduction

Numerical simulation has a potential ability to assist developments in medical research by providing a reliable alternative for decision making by not only providing a low cost decision making tool but also by helping to plan for a medical procedure for future advances. As a result, a wide range of biomedical researches focus on numerical techniques that can aid in these decision support tools. For instance, simulation of blood flow in cardiovascular diseases like aneurysm, thrombosis, stenosis, etc. can lead to a systematic understanding of growth of the disease so as to take appropriate measures to sustain it. It is known that blood flow in these circumstances either aggravates the disease or helps in a systematic cure by a controlled procedure. Though blood is considered to be Newtonian, at low shear rates it resembles to exhibit non-Newtonian behavior and its viscosity happens to be a function of the shear rate. A detailed rheology of blood is discussed in Edward [1]. Blood is also considered to be a complex mixture of cells, proteins and other elements suspended in plasma by Wang and Ho [2], Gijsen et al. [3] and Hron et al. [4]. At low shear rates, these elements are responsible for shear-thinning behavior. Various models like power-law model, Casson model, K-L model, cross model and Carreau-Yasuda model have been proposed to represent blood flow in Wang and Ho [2], Ashrafizaadeh and Bakhshaei [5] of which Casson model has been widely used in the literature. However, the disadvantage of this model is the limited validity of shear rate range which is overcome by Carreau-Yasuda model used by Wang and Benrsdorf [6].

Coupling of these models along with an appropriate numerical technique provides a good simulation tool to understand rheology of blood. Lattice Boltzmann method (LBM), for its kinetic essence and the ability to predict localized fluid properties, fits in to be a better option compared to other numerical techniques. As a result, a large number of researches had focused on using LBM to simulate blood flow. Ouared and Chopard [7] used LBM to simulate non-Newtonian blood flow in stenotic aneurysm using Casson model. They proposed a correction in the method based on the transport

by the plasma of red blood cells as well as an aggregation process starting in the low shear stress regions, near the aneurysm walls. Dupin et al. [8] demonstrated the application on multi-component LBM to simulate mutually immiscible liquid species and blood flow. Bernsdorf and Wang [9] used D3Q19 LBM model to simulate blood flow in cerebral aneurysm in domains created from medical images. This paper considers a porous like square stenotic medium in a human artery with fluid (blood) at the left wall of the geometry and the north wall kept to a normalized temperature of 1.0. The flow properties like velocity profiles, streamlines, temperature profiles and the rate of heat transfer are then studied with respect to the material properties and flow parameters like Rayleigh number and power law index. Porosity is varied from 0.1 to 0.7 whereas is fixed at 10^{-3}. The power law index is varied from 0.5 to 1 to consider shear-thinning behavior of blood and the *Pr* is taken as 4, while *Ra* is varied from 10^3 to 10^5.

2. Numerical Method and Implementation

2.1. Governing equations

The mathematical model for natural convection in porous media can be expressed by the continuity equation, the Brinkman-Forchheimer equation, and the energy equation (Seta et al. [10] and Guo and Zhao [11]):

$$\nabla . u = 0, \tag{1a}$$

$$\frac{\partial u}{\partial t} + (u.\nabla)\left(\frac{u}{\varepsilon}\right) = -\frac{1}{\rho}\nabla(\varepsilon p) + v_e \nabla^2 u + F, \tag{1b}$$

$$\frac{\partial(\rho e)}{\partial t} + \nabla.(\rho u e) = \lambda_{eff}\nabla^2(\rho e). \tag{1c}$$

The total body force is given by

$$F = -\frac{\varepsilon \nu}{K}u - \frac{\varepsilon F_\varepsilon}{\sqrt{K}}|u|u + \varepsilon G. \tag{2}$$

Forchheimer's term F_ε is related to ε as described by Ergun [12]

$$F_\varepsilon = \frac{1.75}{\sqrt{150\varepsilon^3}}, \quad K = \frac{\varepsilon^3 d_p^2}{150(1-\varepsilon)^2}. \tag{3}$$

2.2. Lattice Boltzmann method

The LBM originates from the lattice-gas automata method, in which the fluid is modelled by a single-particle distribution function $f_i(x, t)$ governed by a lattice Boltzmann equation (Seta et al. [10] and Guo and Zhao [11])

$$f_i(x + e_i dt, t + dt) - f_i(x, t) = \frac{f_i^{eq}(x, t) - f_i(x, t)}{\tau} + dtF_i, \tag{4}$$

where υ is given by

$$\upsilon = c_s^2 dt\left(\tau - \frac{1}{2}\right), \tag{5}$$

$f_i^{eq}(x, t)$ is the equilibrium distribution function for D2Q9 given by Guo and Zhao [11]

$$f_i^{eq}(x, t) = w_i\rho(x, t)\left[1 + \frac{1}{c_s^2}(e_i.u(x, t)) + \cdots + \frac{1}{2\varepsilon c_s^4}(e_i.u(x, t))^2 - \frac{u(x, t)^2}{2\varepsilon c_s^2}\right], \tag{6}$$

w_i is the weight coefficient with the values

$$w_i = \begin{cases} 4/9 & i = 0 \\ 1/9 & i = 1, 2, 3, 4 \\ 1/36 & i = 5, 6, 7, 8. \end{cases} \tag{7}$$

The force term F_i is given by

$$F_i = w_i\rho\left(1 - \frac{1}{2\tau}\right)\left[\frac{e_i.F}{c_s^2} + \frac{uF : (e_i e_i - c_s^2 I)}{\varepsilon c_s^2}\right]. \tag{8}$$

The fluid velocity u is given by

$$u = \frac{u_t}{c_0 + \sqrt{c_0^2 + c_1 |u_t|}}, \tag{9}$$

where

$$u_t = \sum_i e_i f_i + \frac{dt}{2} \rho \varepsilon G. \tag{10}$$

The two parameters are given by

$$c_0 = \frac{1}{2}\left(1 + \varepsilon \frac{dt}{2} \frac{v}{K}\right), \quad c_1 = \varepsilon \frac{dt}{2} \frac{F_E}{\sqrt{K}}. \tag{11}$$

2.3. Energy equation

The thermal lattice BGK model is given by Chen and Doolen [13]

$$g_i(x + e_i dt, t + dt) - g_i(x, t) = \frac{g_i^{eq}(x, t) - g_i(x, t)}{\tau_g}. \tag{12}$$

The equilibrium distribution function is given by (Zhao et al. [14] and Nithiarasu et al. [15])

$$g_0^{eq}(x, t) = -\frac{2\rho\varepsilon}{3} \frac{u^2}{c_s^2}, \tag{13a}$$

$$g_i^{eq}(x, t) = \frac{\rho\varepsilon}{9}\left[\frac{3}{2} + \frac{3}{2}\frac{e_i.u}{c_s^2} + \frac{9}{2}\frac{(e_i.u)^2}{c_s^4} - \frac{3}{2}\frac{u^2}{c_s^2}\right] \quad (i = 1, 2, 3, 4), \tag{13b}$$

$$g_i^{eq}(x, t) = \frac{\rho\varepsilon}{36}\left[3 + \frac{6}{2}\frac{e_i.u}{c_s^2} + \frac{9}{2}\frac{(e_i.u)^2}{c_s^4} - \frac{3}{2}\frac{u^2}{c_s^2}\right] \quad (i = 5, 6, 7, 8). \tag{13c}$$

2.4. Boundary conditions and numerical implementation

Second order bounce-back rule for non-equilibrium distribution function f_i is used to determine the velocity on four walls. The distribution functions are given by (Zou and He [16])

$$f_{\alpha}^{neq} = f_{\beta}^{neq}, \tag{14}$$

where β is the opposite direction of α. For energy distribution function g_i, second order extrapolation rule is used on the right wall and the energy distribution function at all other walls is determined with the boundary conditions for all other walls defined as (Mohamad [17])

$$g_{\alpha} = T_w(w_{\alpha} + w_{\beta}) - g_{\beta}. \tag{15}$$

Carreau-Yasuda model is used to represent non-Newtonian fluids given by (Sochi [18])

$$\mu = \mu_0 + (\mu_0 - \mu_{\infty})/(1 + a(\dot{\gamma})^b)^{\frac{n-1}{b}}, \tag{16}$$

where μ_0 and μ_{∞} are the viscosities at zero and infinite shear rate, respectively. The parameters *a* and *b* along with μ_0 and μ_{∞} should be appropriately defined for numerical simulation to converge which depend on index *n* and material properties of the porous media.

3. Results and Discussion

For non-Newtonian fluids, Darcy's law for fluid flowing through a porous media is given by (Sullivan et al. [19])

$$q = \left(\frac{K}{\mu_{eff}} \frac{\nabla p}{L} \right)^{1/n}. \tag{17}$$

Thus, the validity of the numerical procedure for non-Newtonian numerical simulation can be established by verifying that the plot of q and $\nabla p = grad(p)$ is linear with slope $1/n$ as given in Table 1. The values of parameter for 0.5, 0.75 and 1 of μ_0 were identified as 0.1, 0.06 and 0.02, respectively, while μ_{∞} was fixed at 0.001.

Parameters *a* and *b* were taken as 2 and 0.64, respectively. Boundary conditions based on non-equilibrium parts were implemented on velocity

distribution function, while the unknown energy distribution functions were determined as (Yang et al. [20])

$$g_\alpha = T_w(w_\alpha + w_\beta) - g_\beta. \tag{18}$$

The temperature difference between top wall and the fluid induces fluid flow inside the geometry which results in heat transfer. Various flow properties are recorded to quantify the influence of natural convection on these parameters. The *u*-velocity profiles in Figure 1 present the variation in *u*-velocities with respect to *n* for fixed values of ε and *Ra* at the centre half of the cavity. The profiles show a sinusoidal behaviour with the highest velocity magnitude at geometric centre of the cavity. The *u*-velocities were observed to increase in magnitude with *n*, although the basic trend remains the same. Influence of ε and *Ra* is also observed on velocity profiles as ε is increased from 0.4 to 0.7 and *Ra* from 10^3 to 10^5, which can be seen in Figures 1 and 2. These results indicate that an induced flow can help in transporting the saturated particles within the stenosis to move out from the infected part. Plots in Figures 3-8 show the influence of these various flow parameters on streamlines.

Streamlines are symmetric as required for natural convection in a differentially heated geometry. At higher *Ra* values, flow strength is stronger as compared to lower values. Also, as *n* increases from 0.5 to 1, circulation is observed to shift towards the left wall of the cavity. Formation of vortices can be observed for lower values of *Ra* implicating the flow circulation due to dominance of conduction over conduction. As the influence of convection starts dominating, the flow field expands to major part of the geometry. For lower values of *Ra*, vortices on the left of the geometry tend to occupy a bigger space. However, these vortices shift towards left and disappear as flow is influenced by buoyancy effect for higher values of *Ra*. As *n* increases from 0.5 to 1, the flow field due to convection increases which is relevant form expansion of flow field from right to left.

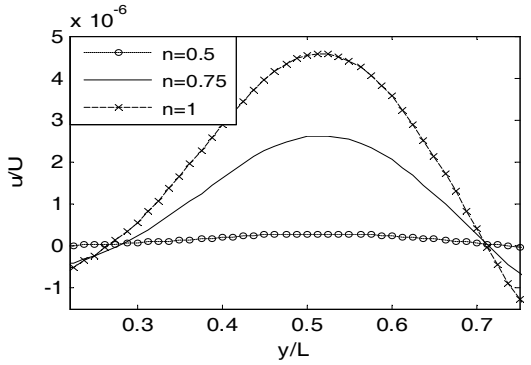

(a)

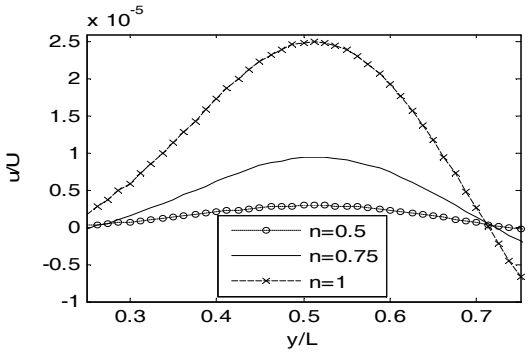

(b)

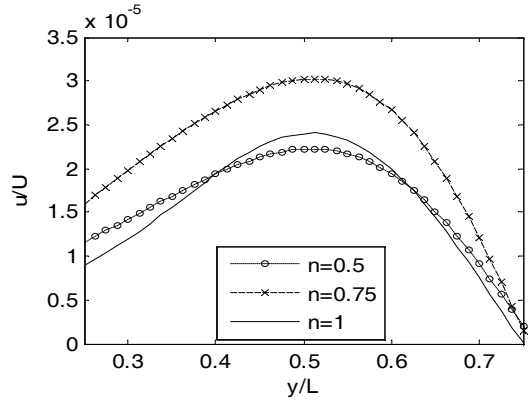

(c)

Figure 1. *u*-velocity profiles for $\varepsilon = 0.4$ at various values of n: (a) $Ra = 10^3$, (b) $Ra = 10^4$ and (c) $Ra = 10^5$.

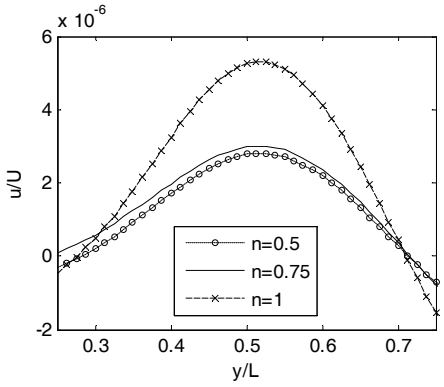

(a)

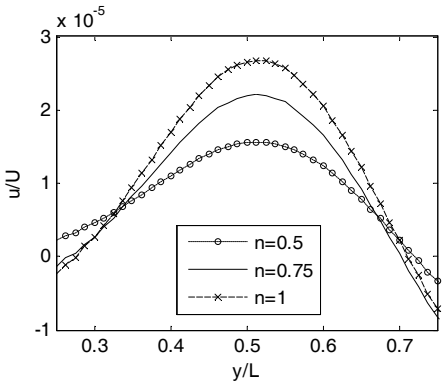

(b)

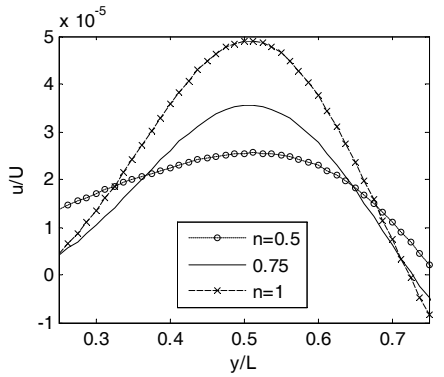

(c)

Figure 2. *u*-velocity profiles for $\varepsilon = 0.7$ at various values of *n*: (a) $Ra = 10^3$, (b) $Ra = 10^4$ and (c) $Ra = 10^5$.

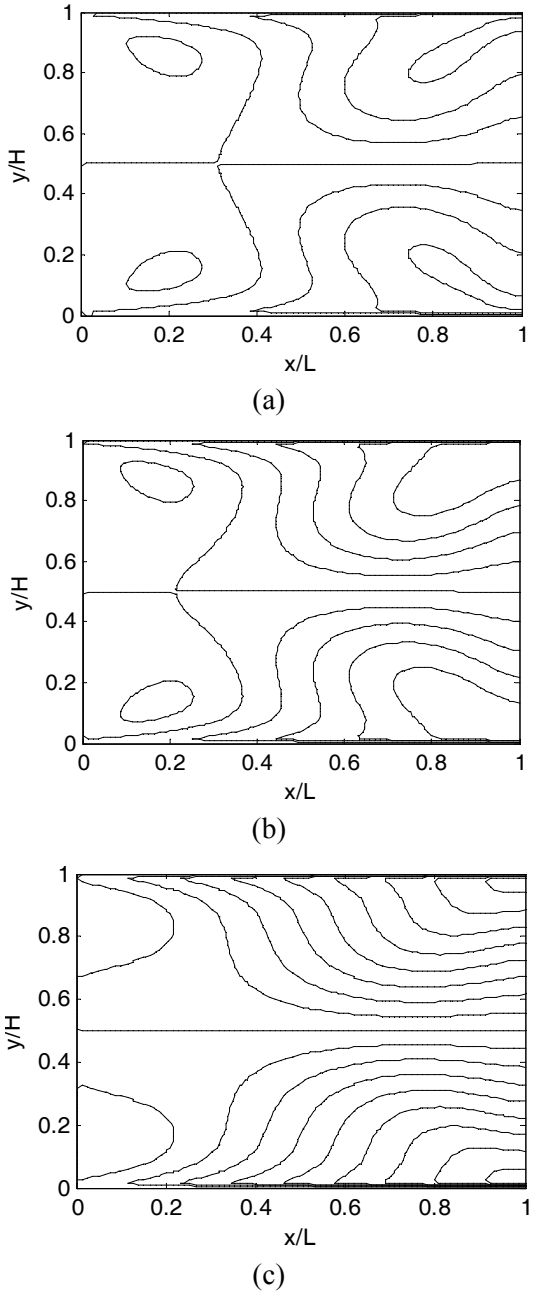

Figure 3. Streamline plots for $n = 0.5$, $\varepsilon = 0.4$: (a) $Ra = 10^3$, (b) $Ra = 10^4$ and (c) $Ra = 10^5$.

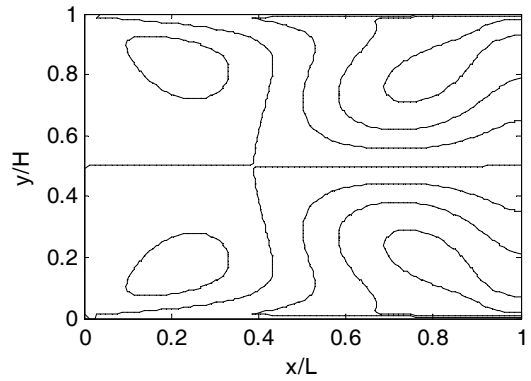

(a)

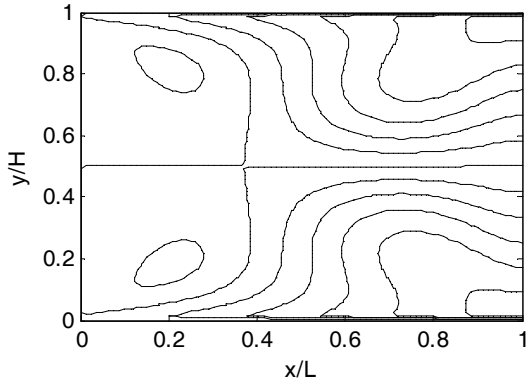

(b)

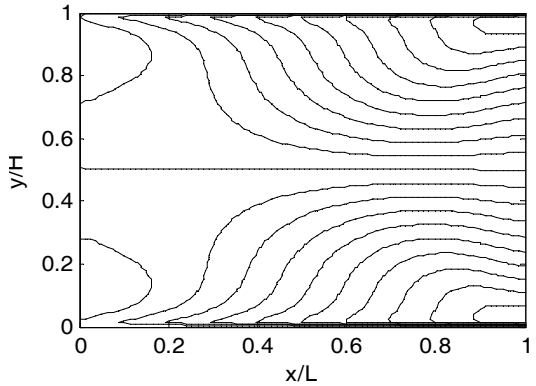

(c)

Figure 4. Streamline plots for $n = 0.75$, $\varepsilon = 0.4$: (a) $Ra = 10^3$, (b) $Ra = 10^4$ and (c) $Ra = 10^5$.

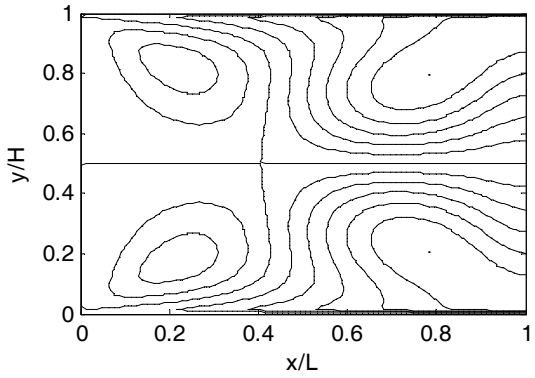

(a)

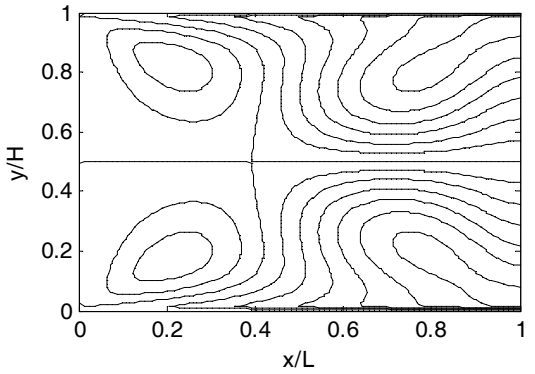

(b)

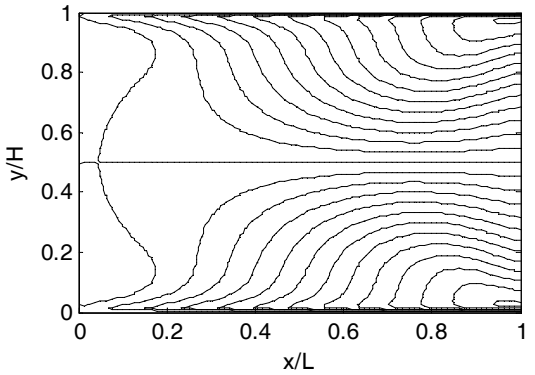

(c)

Figure 5. Streamline plots for $n = 1$, $\varepsilon = 0.4$: (a) $Ra = 10^3$, (b) $Ra = 10^4$ and (c) $Ra = 10^5$.

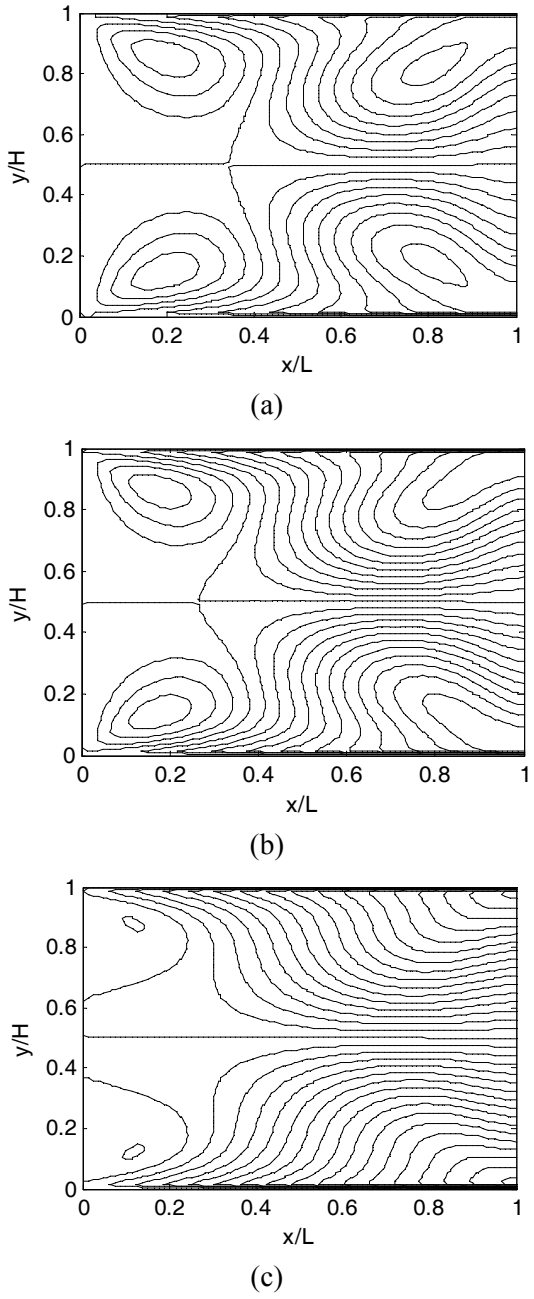

Figure 6. Streamline plots for $n = 0.5$, $\varepsilon = 0.7$: (a) $Ra = 10^3$, (b) $Ra = 10^4$ and (c) $Ra = 10^5$.

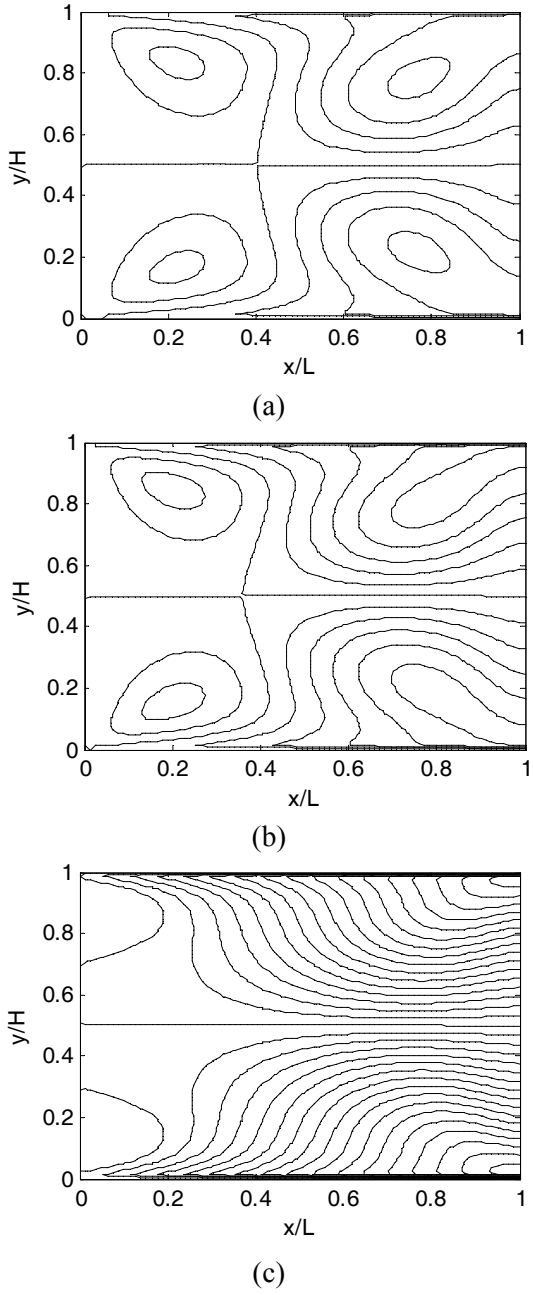

Figure 7. Streamline plots for $n = 0.75$, $\varepsilon = 0.7$: (a) $Ra = 10^3$, (b) $Ra = 10^4$ and (c) $Ra = 10^5$.

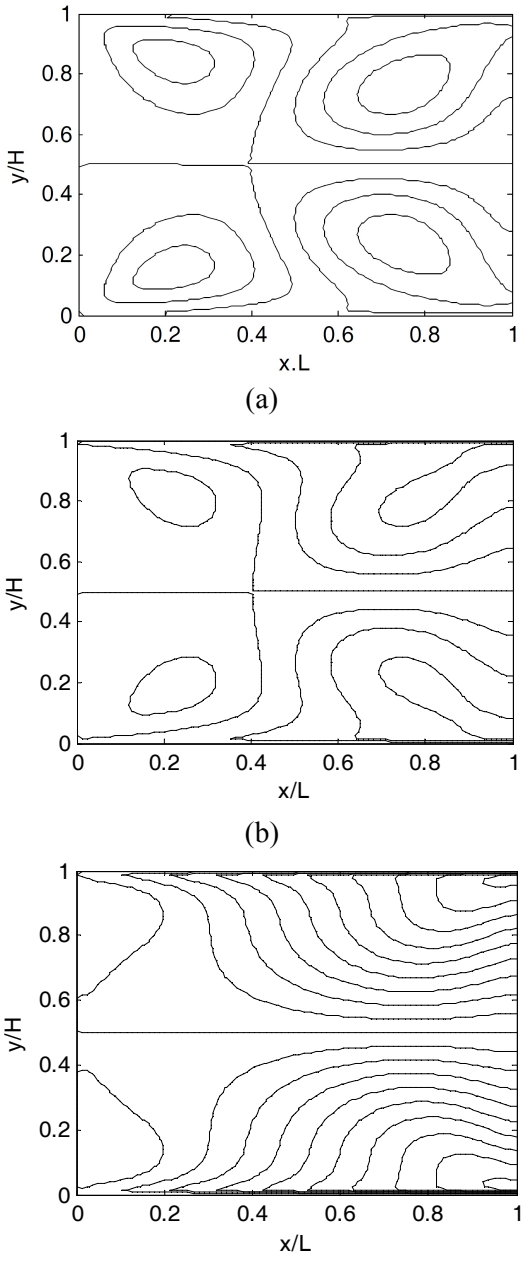

Figure 8. Streamline plots for $n = 1,\ \varepsilon = 0.7$: (a) $Ra = 10^3$, (b) $Ra = 10^4$ and (c) $Ra = 10^5$.

Table 1. *Nu* at hot wall for various values of n, ε and *Ra*

n	$\varepsilon = 0.4$			$\varepsilon = 0.7$		
	Ra			*Ra*		
	10^3	10^4	10^5	10^3	10^4	10^5
0.5	1.3154	1.3169	1.3357	1.3179	1.3205	1.3391
0.75	1.3104	1.3157	1.3274	1.3132	1.3168	1.3299
1	1.3029	1.3140	1.3261	1.3039	1.3144	1.3264

Table 2. Values of τ for various values of n, ε and *Ra*

n	$\varepsilon = 0.4$			$\varepsilon = 0.7$		
	Ra			*Ra*		
	10^3	10^4	10^5	10^3	10^4	10^5
0.5	0.5956	0.5755	0.5287	0.5948	0.5735	0.5278
0.75	0.6021	0.5858	0.5421	0.6009	0.5847	0.5403
1	0.5600	0.5600	0.5600	0.5600	0.5600	0.5600

Better results can be achieved by considering hot and cold treatments alternately for higher temperature difference to increase the velocity of the fluid. Variations in *Nu* values at hot wall are recorded in Table 1 and the average values of the relaxation parameter for various values of n are recorded in Table 2. The rate of heat transfer increases with an increase in porosity and decreases with an increase in power law index. That is because of the shear-thinning behaviour of fluid whose viscosity decreases with shear strain, thus, helping in increased flow strength, eventually, increasing the rate of heat transfer. This process can also be used in pain relief by influencing blood flow in any injured part of the body. Same procedure is followed in natural treatments like naturopathy in which higher temperatures (in terms of warm water or steam) are used to induce a mixed convection.

4. Conclusion

The rate of heat transfer increases with an increase in porosity and decreases with an increase in power law index. The process of increasing rate of heat transfer can be used in pain relief by influencing blood flow in any injured part of the body. At higher *Ra* values, flow strength is stronger as compared to lower values.

With advanced medicinal technology and elevating cost, there is a need of significant research in India to investigate the significance of naturopathy, and thus, hydrotherapy. Since the process in our article is drugless, and thus, have no side effects, a systematic planning and research is necessary to look for a better, cheaper and reliable alternate medical processes. These results shall give an insight into the medical process, mathematically, which will help in making significant improvements in the methods followed. This will help in developing these medical practices as an alternative to the existing medical processes to reduce the ever-increasing medical costs in India. This process can also be used in pain relief by influencing blood flow in any injured part of the body. Same procedure is followed in natural treatments like naturopathy in which higher temperatures (in terms of warm water or steam) are used to induce a mixed convection.

References

[1] Merrill W. Edward, Rheology of blood, Physiological Reviews 49(4) (1969), 1-26.

[2] Chen-Hao Wang and Jeng-Rong Ho, A lattice Boltzmann approach for the non-Newtonian effect in the blood flow, Comput. Math. Appl. 62 (2011), 75-86.

[3] F. J. H. Gijsen, F. N. van de Vosse and J. D. Janssen, The influence of the non-Newtonian properties of blood on the flow in large arteries: steady flow in a carotid bifurcation model, Journal of Biomechanics 32 (1999), 601-608.

[4] J. Hron, J. Málek and S. Turek, A numerical investigation of flow of shear-thinning fluids with applications to blood rheology, Internat. J. Numer. Methods Fluids 32(7) (2000), 863-879.

[5] Mahmud Ashrafizaadeh and Hani Bakhshaei, A comparison of non-Newtonian models for lattice Boltzmann blood flow simulations, Comput. Math. Appl. 58 (2009), 1045-1054.

[6] Dinan Wang and Jörg Bernsdorf, Lattice Boltzmann simulation of steady non-Newtonian blood flow in a 3D generic stenosis case, Comput. Math. Appl. 58 (2009), 1030-1034.

[7] Rafik Ouared and Bastien Chopard, Lattice Boltzmann simulations of blood flow: non-Newtonian rheology and clotting processes, J. Stat. Phys. 121 (2005), 209-221.

[8] M. M. Dupin, I. Halliday and C. M. Care, A multi-component lattice Boltzmann scheme: towards the mesoscale simulation of blood flow, Medical Engineering and Physics 28 (2006), 13-18.

[9] J. Bernsdorf and D. Wang, Non-Newtonian blood flow simulation in cerebral aneurysms, Comput. Math. Appl. 58 (2009), 1024-1029.

[10] Takeshi Seta, Eishun Takegoshi and Kenichi Okui, Lattice Boltzmann simulation of natural convection in porous media, Math. Comput. Simulation 72 (2006), 195-200.

[11] Zhaoli Guo and T. S. Zhao, Lattice Boltzmann model for incompressible flows through porous media, Phys. Rev. E 66 (2002), 036304-1-036304-9.

[12] S. Ergun, Flow through packed columns, Chemical Engineering Process 48 (1952), 89-94.

[13] Shiyi Chen and Gary D. Doolen, Lattice Boltzmann method for fluid flows, Annu. Rev. Fluid Mech. 30 (1998), 329-364.

[14] C. Y. Zhao, L. N. Dai, G. H. Tang, Z. G. Qu and Z. Y. Li, Numerical study of natural convection in porous media (metals) using lattice Boltzmann method (LBM), International Journal of Heat and Fluid Flow 31 (2010), 925-934.

[15] P. Nithiarasu, K. N. Seetharamu and T. Sundararajan, Natural convective heat transfer in a fluid saturated variable porosity medium, Int. J. Heat Mass Transfer 40 (1997), 3955-3967.

[16] Qisu Zou and Xiaoyi He, On pressure and velocity boundary conditions for the lattice Boltzmann BGK model, Phys. Fluids 9(6) (1997), 1591-1598.

[17] A. A. Mohamad, Meso and macro-scales fluid flow simulations with lattice Boltzmann method, The 4th International Symposium on Fluid Machinery and Fluid Engineering, Beijing, China, 24-27 Nov., 2008.

[18] Taha Sochi, Non-Newtonian flow in porous media, Polymer 51 (2010), 5007-5023.

[19] S. P. Sullivan, L. F. Gladden and M. L. Johns, Simulation of power-law flow through porous media using lattice Boltzmann techniques, J. Non-Newtonian Fluid Mech. 133 (2006), 91-98.

[20] Fan Yang, Xuming Shi, Xueyan Guo and Qingyi Sai, MRT lattice Boltzmann schemes for high Reynolds number flow in two-dimensional lid-driven semi-circular cavity, Energy Procedia 16 (2012), 639-644.